European Polymer Journal 198 (2023) 112403

Contents lists available at ScienceDirect

European Polymer Journal

journal homepage: www.elsevier.com/locate/europolj

Advanced 3D printing of graphene oxide nanocomposites: A new initiator system for improved dispersion and mechanical performance

Klaudia Trembecka-Wójciga [a], Magdalena Jankowska [b], Wiktoria Tomal [b], Anna Jarzębska [a], Łukasz Maj [a], Tomasz Czeppe [a], Paweł Petrzak [a], Anna Chachaj-Brekiesz [c], Joanna Ortyl [b,d,e,*]

[a] Institute of Metallurgy and Materials Science, Polish Academy of Sciences, Reymonta 25, 30-059 Cracow, Poland
[b] Department of Biotechnology and Physical Chemistry, Faculty of Chemical Engineering and Technology, Cracow University of Technology, Warszawska 24, 30-155 Cracow, Poland
[c] Faculty of Chemistry, Jagiellonian University, Gronostajowa 2, 30-387 Cracow, Poland
[d] Photo4Chem Lea 114, 30-133 Cracow, Poland
[e] Photo HiTech Ltd, Bobrzynskiego 14, 30-348 Cracow, Poland

ARTICLE INFO

Keywords:
Photopolymerization
3D printing
Photoinitiators
Polymer nanocomposites
Graphene oxide

ABSTRACT

The integration of nanoparticles, such as Graphene Oxide (GO), with photo-curable polymers in 3D printing has garnered significant interest in recent years due to the potential to create functional nanocomposite materials. This study explores the challenges of achieving optimal dispersion of GO nanoparticles within the polymer matrix and the crucial role of photoinitiators in overcoming these limitations. Traditional photoinitiators, like TPO, commonly used for GO/polymer resins, have raised concerns about high toxicity and limited sensitivity to visible light, prompting the need for alternative initiating systems. In this research, we propose a two-component initiator system based on bis-(4-t-butylphenyl)iodonium hexafluorophosphate and photosensitizer N-{4-[(E)-2-(pentafluorophenyl)ethenyl]phenyl}-2,1,3-benzothiadiazol-4-amine (IOD/PS1) as a promising solution. This new initiating system not only ensures a more environment-friendly resin but also exhibits enhanced polymerization kinetics and compatibility with GO nano fillers. This study investigated the effect of the addition of nano-GO on the kinetics of the radical photopolymerization process, 3D printing, and final mechanical and thermal properties of the received products. TPO and PEGDA/H2O were used as reference systems. In addition, a new two-component initiator system was synthesized, which is an interesting alternative to the commercial TPO initiator that is widely employed in additive techniques. This publication presents the research procedure involving various techniques: real-time FTIR and photoreology. In addition, the possibility of creating three-dimensional structures from the newly developed photo-curable resins was verified. Finally, the morphologies and mechanical properties of the resulting 3D structures were compared. Within the work, we demonstrate the advantages of the two-component initiator in achieving uniform distribution of GO and fabricating high-quality materials. By applying IOD/PS1 initiating system we facilitated a more controlled and efficient polymerization process, reducing shrinkage-induced stresses and enhancing interlayer bonding. The result was the fabrication of high-quality, well-dispersed materials with tailored properties suitable for various applications, particularly in the biomedical field.

1. Introduction

Additive manufacturing of polymers with nanoparticles using Digital Light Processing (DLP) is a relatively new area of research that has attracted significant attention in recent years [1–3]. DLP is a type of 3D printing technology that uses a digital light projector to cure liquid resin into solid objects layer by layer [4–8]. This technique offers high resolution, speed, and accuracy, making it an attractive option for various applications including biomedical engineering [9–11]. Using this technique, liquid resin can be easily mixed with a variety of nanofillers for the manufacture of functional nanocomposite materials [12–14]. Nanofillers incorporation in a polymer matrix can improve the

* Corresponding author at: Department of Biotechnology and Physical Chemistry, Faculty of Chemical Engineering and Technology, Cracow University of Technology, Warszawska 24, 30-155 Cracow, Poland.
E-mail address: jortyl@pk.edu.pl (J. Ortyl).

https://doi.org/10.1016/j.eurpolymj.2023.112403
Received 31 July 2023; Received in revised form 23 August 2023; Accepted 30 August 2023
Available online 1 September 2023

mechanical and thermal properties of the final material [15–19]. On the other hand, the introduction of nanoadditives to the polymer resin may disturb the photoinduced polymerization processes and thus limit the printability and quality of the printouts. Therefore, selecting a proper photoinitiator becomes a key factor in ensuring the efficient and uniform cross-linking of the printed material, especially when incorporating components that are not inherently permeable to light, such as nano-scale additives like Graphene Oxide (GO).

The use of proper initiating systems is of paramount importance to overcome the limitations associated with the incorporation of GO nano fillers into photo-curable resin [20–22]. When nanoadditives like GO are introduced into the resin matrix, they can significantly influence the photoinduced polymerization processes due to their unique physico-chemical properties [23–24]. Without an appropriate initiating system, the dispersion and interaction of GO within the resin can be compromised, leading to uneven curing, poor mechanical properties, and reduced print quality [25–27]. A well-selected photoinitiator plays a crucial role in promoting uniform cross-linking and efficient curing of the resin, particularly when incorporating non-permeable nano-scale components like GO [28–30]. The photoinitiator's ability to initiate the polymerization reaction and generate reactive species upon exposure to light ensures proper curing throughout the resin, including regions containing GO nano fillers [31–32]. An effective initiating system can enhance the dispersion and compatibility of GO nanoparticles within the resin matrix, minimizing agglomeration and improving the mechanical performance of the printed material. Additionally, it can mitigate issues related to shrinkage mismatch and reduce the risk of cracks or defects in the final printouts [33–35]. By using the appropriate initiating system, researchers can harness the full potential of GO nano fillers to enhance the material properties of the resin-based composite. This includes achieving improved mechanical strength [36–37], enhanced thermal stability [38], and better electrical conductivity [39–40], opening up new avenues for advanced engineering applications.

So far, researchers have made notable efforts to address the challenge of achieving optimal dispersion of GO particles within various matrices. The uniform distribution of GO nanoparticles in the resin matrix is a critical factor in determining the final properties and performance of the composite material [41–42]. A well-dispersed GO network ensures efficient load transfer and enhances mechanical, thermal, and electrical properties. To improve the dispersion of GO particles, scientists have explored several approaches. One common method involves modifying the surface functional groups of GO through chemical functionalization [43–44]. Functionalization alters the interactions between GO and the matrix, reducing agglomeration and enhancing compatibility [45]. This approach has shown promise in improving the dispersion of GO and promoting a homogeneous distribution within the resin. Another technique employed is the use of prolonged sonication during the mixing process [46–48]. Sonication helps to disperse and exfoliate GO sheets, breaking down large agglomerates into smaller, well-dispersed nanoparticles [49]. This mechanical dispersion method has demonstrated some success in achieving more uniform distribution, but it may also introduce additional challenges such as potential damage to GO structure or the need for extended processing times [50–52].

In the context of ongoing research, our work presents a novel approach to enhance the dispersion of GO nanoparticles within the resin matrix. Instead of solely relying on surface functionalization or extended sonication, we investigate the influence of high-performance two-component initiator system on the dispersion of GO in the resin. The intiating system, designed with specific chemical properties, exhibits a remarkable ability to facilitate the dispersion of GO and improve compatibility with the resin matrix. Its unique chemical structure enables strong interactions with the functional groups present on the GO surface, reducing the likelihood of agglomeration and promoting uniform distribution throughout the composite.

Traditionally, the most commonly used photoinitiator for GO/polymer resins has been TPO [53]. However, due to concerns about its high toxicity [54] and other limitations like limited sensitivity to visible light and oxygen inhibition during the polymerization process [55–57], there is a growing need to explore alternative initiating systems. In this regard, our research presents a highly promising solution through the use of a two-component initiator system based on bis-(4-t-butylphenyl)iodonium hexafluorophosphate and photosensitizer N-{4-[(E)-2-(pentafluorophenyl)ethenyl]phenyl}-2,1,3-benzothiadiazol-4-amine (IOD/PS1). This innovative initiator system allows us to overcome the drawbacks associated with traditional photoinitiators, achieving a more environment-friendly resin with improved polymerization kinetics and enhanced performance. By leveraging the unique properties of this two-component initiator, we not only achieve more efficient curing and reduced oxygen inhibition but also synergistic effects with GO nano fillers, leading to a significant enhancement in the overall properties of the GO-reinforced resin. This advancement paves the way for the development of advanced nanocomposite materials, offering immense potential for diverse applications in additive manufacturing, biomedicine, electronics, and beyond.

In this study, we prepared composite materials using a combination of Polyethylene glycol diacrylate (PEGDA) and GO, with a commercially available TPO initiator system as the reference material. We conducted a comprehensive investigation of the effects of nano-GO on the kinetic properties, 3D printing process, and thermal and mechanical properties of the achieved polymer structures. To characterize the photo-curable compositions, we performed rheological behavior analysis to assess the flow properties and viscosity of the resin mixtures. Additionally, thermal analysis was conducted to study the curing behavior and thermal stability of the composite materials. Mechanical analysis was employed to evaluate the strength, toughness, and other mechanical properties of the printed structures.FTIR analysis was utilized to gain insights into the chemical interactions and cross-linking processes occurring during the photopolymerization of the PEGDA/GO composites. As an essential aspect of our research, we explored the possibility of replacing the commercially available TPO initiator with a high-performance two-component initiator system (IOD/PS1). This new initiating system was carefully designed and synthesized to address the limitations associated with traditional photoinitiators. Through systematic experimentation, we demonstrated the potential of this two-component initiator system in achieving a uniform distribution of GO within the polymer matrix, resulting in high-quality materials with enhanced properties.

2. Materials and methods

2.1. Materials

A commercially available TPO photoinitiator (diphenyl (2,4,6-trimethyl benzoyl) phosphine oxide, Allnex) was used as the one-component initiator system. In addition, compositions containing a two-component initiator system were prepared: iodonium salt IOD (bis-(4-t-butylphenyl)iodonium hexafluorophosphate, SpeedCure 938, Lambson) and the new photosensitizer PS1 (N-{4-[(E)-2-(pentafluorophenyl)ethenyl]phenyl}-2,1,3-benzothiadiazol-4-amine). The resin formulations contained the following monomers: poly(ethylene glycol) diacrylate (PEGDA, Sigma Aldrich, average Mn 575) and pentaerythritol triacrylate (PETIA, Sigma Aldrich). As a nanoadditive, GO (graphene oxide nanocolloids, 2 mg/ml, dispersion in H_2O, Sigma Aldrich) was selected for the kinetic studies, 3D printing experiments, and strength tests. The radiation absorbing additive in the resin composition was tartrazine (TT dye content $\geq$ 85 %, Sigma Aldrich). Fig. 1 shows the compound structures that have been used as components of the photoinitiating systems.

2.2. Spectroscopic characteristic

A Cary 60 UV–VIS spectrophotometer (Agilent Technologies) with a

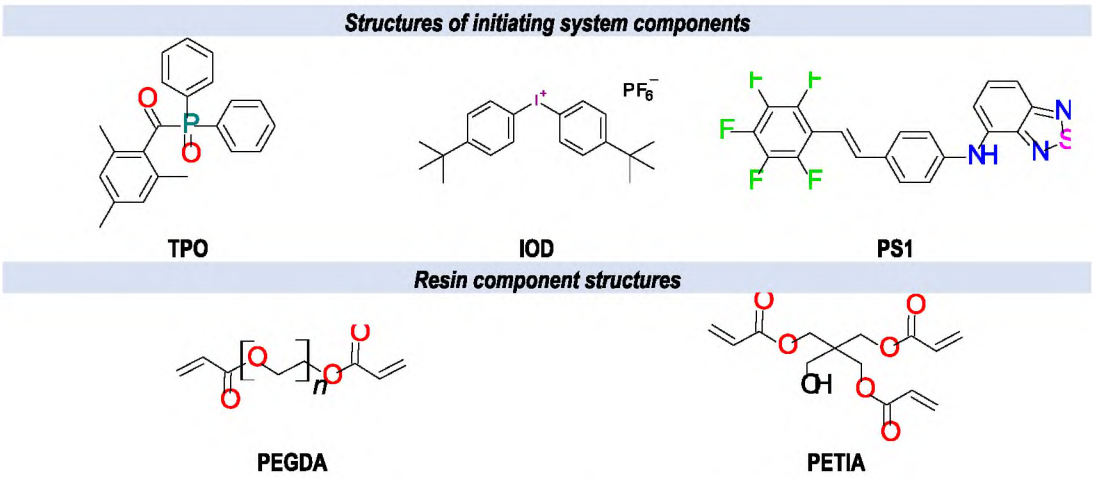

Fig. 1. Structures of initiating system and resin components.

wide spectral range of 190–1100 nm equipped with a xenon flash lamp (80 Hz) was used to determine the spectroscopic properties of the investigated components of the initiating system and the prepared resin formulations.

2.3. Real-time FT-IR measurements

Real-time FT-IR spectroscopy was implemented to determine the initiation efficiencies of the initiating systems. A NICOLET^{TM} iS^{TM} 10 spectrometer (Thermo Fisher Scientific) equipped with a horizontal attachment was employed. LEDs emitting radiation at a wavelength of 405 nm were applied as a light source (M405L4 from Thorlabs with light intensity on the investigated sample: 2.98 mW/cm^2; M405LP1 from Thorlabs with light intensity on the tested sample: 8.82 mW/cm^2). Photopolymerization kinetics by real time FT-IR technology was verified for the following resins: **GO BASE:** GO/PEGDA (3/1 w/w); **GO resin:** TPO/TT (1/0.1 w/w) and GO/PEGDA (37.5/62.5 w/w); **REF1:** TPO (1 % by weight) and PEGDA; **REF2:** TPO/TT (1/0.1 w/w) and PEGDA; **REF3:** TPO (1 % by weight) and H_2O/PEGDA (37.5/62.5 w/w); **REF4:** TPO/TT (1/0.1 w/w) and H_2O/PEGDA (37.5/62.5 w/w); **REF5:** PS1/IOD (0.1/1 w/w) and PETIA/ H_2O/PEGDA (30/26.25/43.75 w/w/w); **GO new resin:** PS1/IOD (0.1/1 w/w) and PETIA/ GO/PEGDA (30/26.25/43.75 w/w/w). The degree of conversion of the functional groups present in the photo-cured resin was determined by the disappearance of the characteristic band for C=C bonds (6120 – 6200 cm^{-1}) [58] employing the following formula:

$$\mathbf{C} = \left(1 - \frac{\mathbf{A}_{\text{after photopolymerization}}}{\mathbf{A}_{\text{before photopolymerization}}}\right) * 100\,[\%] \quad 59.$$

Where:

C = conversion of functional groups [%]; A = area of characteristic bands.

2.4. Rheological behaviour on photo-curable compositions

A modular compact Rheometer MCR302 (Anton Paar) was employed to examine the rheological properties of the prepared photo-cured resins. Measurements were carried out under well-defined conditions: initial thickness of the tested resin 0.1 mm, frequency 1.0 Hz, strain amplitude 1.0 %. Vis LED 405 nm was applied as the light source, the light intensity on the test sample was 2.98 mW/cm^2 (for **GO BASE:** GO/PEGDA (3/1 w/w); **GO resin:** TPO/TT (1/0.1 w/w) and GO/PEGDA (37.5/62.5 w/w); **REF1:** TPO (1 % by weight) and PEGDA; **REF2:** TPO/TT (1/0.1 w/w) and PEGDA; **REF3:** TPO (1 % by weight) and H_2O/PEGDA (37.5/62.5 w/w); **REF4:** TPO/TT (1/0.1 w/w) and H_2O/PEGDA (37.5/62.5 w/w)) and 8.82 mW/cm^2 (for **REF5:** PS1/IOD (0.1/1 w/w) and PETIA/ H_2O/PEGDA (30/26.25/43.75 w/w/w); **GO new resin:** PS1/IOD (0.1/1 w/w) and PETIA/ GO/PEGDA (30/26.25/43.75 w/w/w)), which was measured with a PM160 measuring device (Si Sensor Power Meter, from ThorLabs). Each measurement lasted for 300 s, and the light source was turned on 30 s after the start of the measurement. The temperature of the examination chamber was constant at 25 °C. This study made it possible to determine the gelation time of individual resin compositions and polymerization shrinkage [59,60]. The gelation time was determined from the intersection point of the storage and loss moduli. Polymerization shrinkage was determined using the following formula:

$$\mathbf{S} = \left(1 - \frac{\mathbf{d}_{\text{end}}}{\mathbf{d}_{\text{start}}}\right) * 100\,[\%] \quad 4.$$

Where:

S = polymerization shrinkage [%]; d_{start} = initial sample thickness [mm]; d_{end} = final sample thickness [mm].

2.5. 3D printing experiments

The following photo-curable resins were utilized for DLP 3D printing experiments: **GO resin:** TPO/TT (1/0.1 w/w) and GO/PEGDA (37.5/62.5 w/w); **REF2:** TPO/TT (1/0.1 w/w) and PEGDA; **REF4:** TPO/TT (1/0.1 w/w) and H_2O/PEGDA (37.5/62.5 w/w); **REF5:** PS1/IOD (0.1/1 w/w) and PETIA/ H_2O/PEGDA (30/26.25/43.75 w/w/w); **GO new resin:** PS1/IOD (0.1/1 w/w) and PETIA/ GO/PEGDA (30/26.25/43.75 w/w/w).

2.5.1. Determination of printing parameters

To adequately carry out the 3D printing process, it is necessary to know the optimal parameters, and for this purpose, the prepared resins were tested using Jacob's basic working curves. These experiments allow the determination of the Critical Energy (Ec), which is necessary to initiate the photopolymerization process, as well as the depth of light penetration (Dp). The parameters were determined using the following formula:

$$\mathbf{C_d} = \mathbf{D_p} * \mathbf{ln}\frac{\mathbf{E_0}}{\mathbf{E_c}}\,[\mu m]$$

Where:

Cd = thickness of the cured resin slice [μm]; E_0 = light energy on the investigated sample surface [mJ/cm^2].

From the obtained data, a plot of Cd = f(E_0) was established, from which the critical energy (the intersection point of the plot with the X-axis) and the depth of light penetration (the slope of the resulting curve) were computed. Knowledge of Dp and Ec allows for the selection of

appropriate exposure settings to optimize the printing conditions for the best resolution.

2.5.2. 3D printing using DLP technology

A Lumen X+™ printer was applied to achieve digital light processing prints. The light intensity of the photo-cured resin was 1.99–9.95 mW/cm^2. The 3D printed designs were prepared using Fusion360® software (AutoDesk). The resulting prints were cleaned and postcured in a Wanhao Boxman Curing Chamber (at 405 nm), the post-curing time for each print took 10 and 60 min, respectively.

2.6. Determination of final properties of three-dimensional materials

2.6.1. Microscopic analysis of the resulting materials

Nanoscale observations of as-supplied graphene oxide were carried out using an FEI Tecnai G2 SuperTWIN 200 kV FEG transmission electron microscope equipped with a SIS MegaView III CCD camera for acquisition of microstructure images in bright-field mode (TEM/BF) as well as selected area electron diffraction (SAED) patterns. The samples for TEM studies were prepared on a lacey carbon support. Surface topography observations were carried out using an Axia Thermofisher scanning electron microscope (SEM) at 10 keV in the secondary electron (SEM/SE) mode. To overcome the charge-up effect, the surfaces of the investigated samples were sputter-coated with carbon using a Leica EM SCE 500 deposition system.

2.6.2. Mechanical analysis

The mechanical properties of the tested materials were evaluated via uniaxial compression tests. The compression tests were performed using an INSTRON 6025 modernized by a Zwick/Roell testing machine equipped with static load cells with a small range of compressive forces. The measurements were carried out at room temperature (~23 °C) and at a constant strain rate of 0,1 mm/min. Test specimens were mounted on cylindrical hardened steel dies. Fig. 2 shows a simplified diagram of the deformation process. Three tests were performed for each type of material to maintain appropriate statistics and check the repeatability of the results.

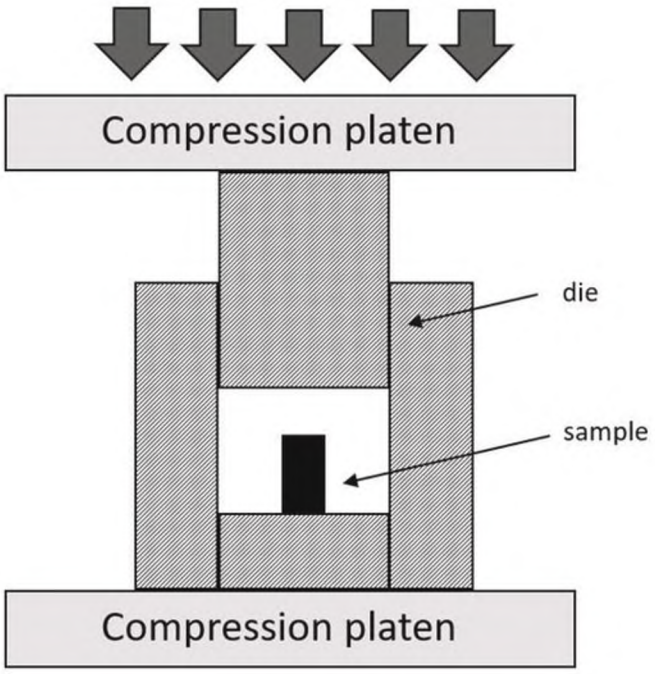

Fig. 2. Simplified diagram of the deformation process.

2.6.3. Thermal analysis

Changes in the thermal stability of PEGDA after the addition of GO nanoparticles were studied. The thermal behavior of PEGDA and PEGDA/GO was analyzed by TGA and DSC. The weight losses during the sample drying stage and the subsequent heating up to 700 °C were measured using thermogravimetric analysis (TGA) by Mettler Toledo, while the heat flow during that process was followed by the differential scanning calorimetry (DSC) method using Q1000 (TA Instruments).

3. Results and discussion

3.1. Spectroscopic characteristic

The main objective of the spectroscopic studies was to determine the effect of GO addition on spectroscopic properties. Therefore, absorption measurements were performed for the following compositions: **GO resin:** TPO/TT (1/0.1 w/w) as the photoinitiating system with GO/PEGDA (37.5/62.5 w/w), and **REF4:** TPO/TT (1/0.1 w/w) as the photoinitiating system with H_2O/PEGDA (37.5/62.5 w/w). Spectroscopic measurements showed that the studied compositions had absorptions up to approximately 500 nm. The GO nanoadditive did not cause any deterioration in the spectroscopic characteristics. Fig. 3 shows the absorption spectra of the GO resin and the REF4 compositions.

3.2. Real-time FTIR measurements

The subsequent research stage involved checking the kinetic properties of the investigated photo-curable resins. To this goal, resins: **GO BASE:** GO/PEGDA (3/1 w/w); **GO resin:** TPO/TT (1/0.1 w/w) and GO/PEGDA (37.5/62.5 w/w); **REF1:** TPO (1 % by weight) and PEGDA; **REF2:** TPO/TT (1/0.1 w/w) and PEGDA; **REF3:** TPO (1 % by weight) and H_2O/PEGDA (37.5/62.5 w/w); **REF4:** TPO/TT (1/0.1 w/w) and H_2O/PEGDA (37.5/62.5 w/w) were analyzed using infrared spectroscopy techniques. Photopolymerization kinetics studies were carried out on 0.1 mm thick rings, which are compatible with the layer thickness of 3D printed objects. Each measurement lasted 900 s, and the light source in the form of a VisLED at @405 nm was turned on after the initial 10 s of the kinetics measurement. The graph below shows the kinetic profiles

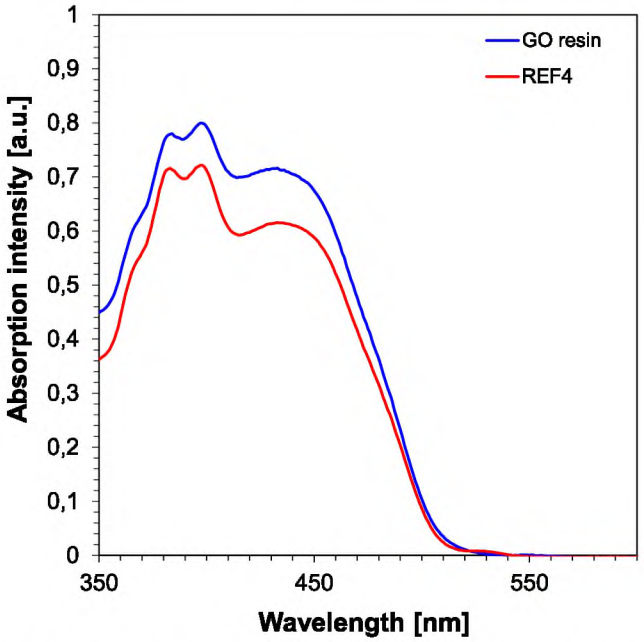

Fig. 3. Absorption spectrum of **GO resin** (TPO/TT/GO/PEGDA 1/0.1/37.5/62.5 w/w/w/w) and **REF4** (TPO/TT/H_2O/PEGDA 1/0.1/37.5/62.5 w/w/w/w).

obtained during radical photopolymerization of the photo-curable formulations examined.

According to the experiments, the conversion rate of the PEGDA acrylate monomer, induction times for each resin, and slope curves were determined. All kinetic parameters are listed in Table 1. where conversion is the final conversion of acrylate groups and dC/dt is a parameter that describes the rate of photopolymerization.

The investigated samples showed that the addition of GO to the photo-curable resin did not have an inhibitory effect on radical photopolymerization kinetics. The obtained conversions of acrylate groups for all resins (except GO BASE, with is the resin without photoinitiating system) were very high and amount to 95–97 %. Nevertheless, in the initial phase of the photopolymerization process, we noticed fundamental differences for the tested samples due to different induction times varying from 12 s to as little as 2 s, and the slope of the kinetic curve in the initial phase of the process was very different, which indicates the various reactivities of the resins. It is mainly related to the fact that the content of the photoinitiating system was applied with the same weight concentration to the total weight of the sample, not just to the weight of the monomer. Therefore, the total initiator concentration per monomer for sample REF1 was 1 % by weight, and for the initiator in sample REF3 is 1.6 % by weight after calculating the mass of monomer contained in the sample. Based on the analysis of the kinetic data presented in Table 1 and Fig. 4, comparing the results for samples REF3 and REF4, it is evident that changing the composition of the photoinitiator system results in changes in the kinetics. The addition of TT to a photo-curable formulation is generally expected to improve the 3D printing parameters to ensure adequate resolution of printed objects. In our case, a slight addition of TT equal to 0.1 % by weight of the sample resulted in a reduction in induction time and acceleration of photopolymerization kinetics in the initial period of monitoring the photopolymerization process. Summarizing the results obtained, it can be said that kinetic parameters for GO resin and REF4 samples were obtained similar, this indicates that GO addition does not have an inhibitory effect on the photopolymerization process under the established test conditions, only slightly the kinetic rate of the photopolymerization process (dC/dt) decreases compared to the REF4 reference sample. The spectra before and after the photopolymerization process for all the studied compositions are included in the Supplement (**S.2.-S.9.**).

3.3. *Rheological behaviour on photo-curable compositions*

Photorheological measurements were performed to determine the polymerization shrinkage of the investigated photo-curable resins. The intensity of 405 nm light on the sample was the same as for FT-IR measurements and was 2.98 mW/cm^2 (for resins: **GO BASE:** GO/PEGDA (3/1 w/w); **GO resin:** TPO/TT (1/0.1 w/w) and GO/PEGDA (37.5/62.5 w/w); **REF1:** TPO (1 % by weight) and PEGDA; **REF2:** TPO/TT (1/0.1 w/w) and PEGDA; **REF3:** TPO (1 % by weight) and H_2O/PEGDA (37.5/62.5 w/w); **REF4:** TPO/TT (1/0.1 w/w) and H_2O/PEGDA (37.5/62.5 w/w)). The results obtained are presented as the dependence of the loss modulus, storage modulus, and normal force on time (graphs are presented in Supplement **S.11.-S.18.**). No changes were observed in the composition of GO BASE over the course of the measurements. The highest polymerization shrinkage was observed for REF1 resin. The value of this parameter for this resin was 6 % (composition without water). For the GO resin and REF3 samples, no polymerization shrinkage was observed under radiation. Based on this study, it was also possible to determine the gelation times of the individual compositions. The determined times were very short, indicating that the process occurred very quickly. The calculated values of gelation time and polymerization shrinkage are listed in Table 2.

3.4. *3D printing of composite materials*

3.4.1. *Determination of printing parameters*

Characteristic printing parameters, such as the critical energy and light penetration depth, were determined from Jacob's basic working curves. For each resin, which were utilized in subsequent 3D printing work, an analysis of printing parameters was carried out, the selected samples for research were: **REF2** (TPO/TT (1/0.1 w/w) and PEGDA), **REF4** (TPO/TT (1/0.1 w/w) and H_2O/PEGDA (37.5/62.5 w/w)) and **GO resin** (TPO/TT (1/0.1 w/w) and GO/PEGDA (37.5/62.5 w/w)). For Jacob's basic working curves, nine slices measuring 1 × 1 cm were printed at different times. The thickness of each slice was measured five times using a micrometer screw, and the average thickness value was determined. The E_0 value shown in the graph corresponds to the quotient of the exposure time of a given slice and power of the printer. The Cd parameter in Fig. 5 represents the thickness of the cured resin.

The critical energy and depth of light penetration were determined according to the experiments, as shown in Table 3. As can be seen, the addition of GO to the photopolymerization resin results in a decrease in the critical energy value, as well as a decrease in the light penetration depth value compared to the reference resins. From the results obtained, it can be seen that GO resin with GO (0.075 % by weight) exhibits the lowest critical energy value, i.e. the lowest amount of energy required to supply the system for the photopolymerization to occur in an object of a given thickness. This phenomenon may indicate a potentially accelerating effect of GO on the photopolymerization process. Nevertheless, by analyzing the second determined parameter, it can be seen that with the addition of GO to the sample, the depth of light penetration decreases drastically, which is completely reasonable considering the absorption properties of graphene oxide in a 100 um thick printed layer.

3.4.2. *3D printing using DLP technology*

Based on the results obtained from the analysis of the printing parameters and monitoring the photopolymerization processes using online techniques, we attempted to print objects with specific morphologies and shapes. Subsequently, the DLP 3D printing experiments were performed. The following resins were used for the experiments: **GO resin:** TPO/TT (1/0.1 w/w) and GO/PEGDA (37.5/62.5 w/w); **REF2:** TPO/TT (1/0.1 w/w) and PEGDA; **REF4:** TPO/TT (1/0.1 w/w) and H_2O/PEGDA (37.5/62.5 w/w). Three-dimensional objects were prepared for further research. 3D structures were prepared and used for microscopic resolution investigations, and printed cylinders were prepared, which served as the test material for the strength tests (Fig. 6). Table 4 lists the printing parameters for each resin.

Table 1
Kinetic parameters obtained during radical photopolymerization under 405 nm (Light intensity on photopolymerizing composition = 2.98 mW/cm^2).

Resin	Composition	Conversion [%]	Induction time [s]	dC/dt
GO BASE	GO/PEGDA (3/1 w/w)	No polymerization	No induction time	–
GO resin	TPO/TT (1/0.1 w/w) and GO/PEGDA (37.5/62.5 w/w)	95	2.22	4.29
REF1	TPO (1 % by weight) and PEGDA	96	11.76	2.29
REF2	TPO/TT (1/0.1 w/w) and PEGDA	97	12.25	2.25
REF3	TPO (1 % by weight) and H_2O/PEGDA (37.5/62.5 w/w)	96	8.86	6.46
REF4	TPO/TT (1/0.1 w/w) and H_2O/PEGDA (37.5/62.5 w/w)	95	2.05	6.76

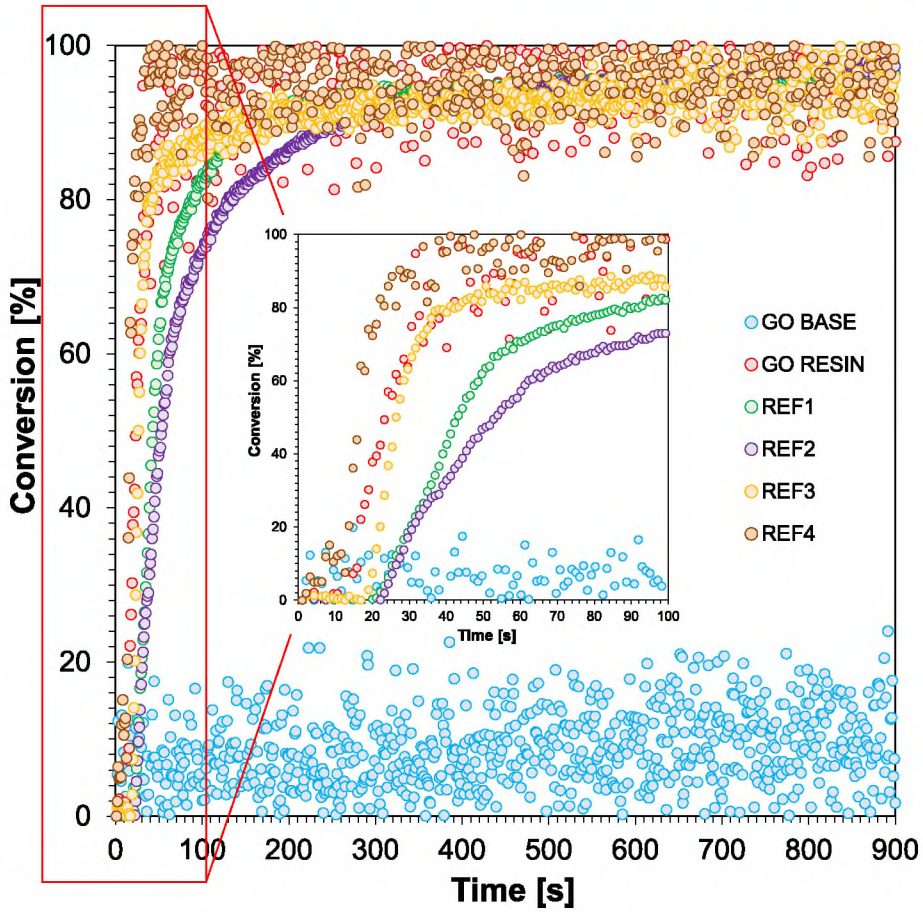

Fig. 4. Kinetic profiles obtained during radical photopolymerization for resins with a one-component initiator system.

Table 2
Determined values of gelation time and polymerization shrinkage for photo-curable resins under 405 nm (Light intensity on photopolymerizing composition = 2.98 mW/cm^2).

Resin	Composition	Gel time [s]	Polymerization shrinkage [%]
GO BASE	GO/PEGDA (3/1 w/w)	No polymerization	No polymerization
GO resin	TPO/TT (1/0.1 w/w) and GO/PEGDA (37.5/62.5 w/w)	0.35	0
REF1	TPO (1 % by weight) and PEGDA	1.50	6
REF2	TPO/TT (1/0.1 w/w) and PEGDA	3.90	5
REF3	TPO (1 % by weight) and H_2O/PEGDA (37.5/62.5 w/w)	0.37	0
REF4	TPO/TT (1/0.1 w/w) and H_2O/PEGDA (37.5/62.5 w/w)	0.93	2

3.5. *Determination of final properties of three-dimensional materials*

3.5.1. *Surface analysis*

A TEM/BF microstructure image of the as-supplied graphene oxide flakes is shown in Fig. 7. One may distinguish folded sheets of material (several micrometers long) that are free from contaminants. The semi-transparency of the material for the electron beam and the lack of visibility of the edges of the flakes suggest the presence of many layers of stacked material. The SAED pattern acquired from the area also covering part of the folded graphene oxide presents continuous rings of intensity overlapped with distinct spots (Fig. 7b). Indexing of the SAED pattern allowed us to prove the graphite phase (the spot diffraction pattern corresponds to [0001]C).

The morphologies of REF1, REF4, and the GO resin composite observed using scanning electron microscopy (SEM) are shown in Fig. 8. Print fidelity and dimensions changed when the material composition was changed. According to the results, the reference samples exhibited weak structural integrity in comparison to materials with GO particles. Among the studied reference combinations, samples with higher PEGDA concentrations showed better printing fidelity. The printing accuracy decreased with increasing water content of the PEGDA hydrogel. When the PEGDA concentration was reduced, the printing accuracy decreased because a lower PEGDA concentration led to a reduced crosslinking degree and negatively affected the printability of the fine structure. The addition of GO particles improves the quality of the printouts, regardless of the addition of water to the resin. This indicates a strong interaction between the polymer chain and GO particles [61]. Within the material, sequencing of the surface relief appeared, which proved the homogeneous dispersion of GO in the material.

The degree of curing is critical for the structure fabricated via digital light processing [62], as shown in Fig. 8. For the control samples, extending the curing time resulted in crack propagation along the material. Increasing the curing time enabled GO to scatter closer to the remaining monomers, making the structure more compact. Thus, much greater differences in the mesh dimensions are visible. The width of the final layers is almost two times smaller for GO resin 60 min sample

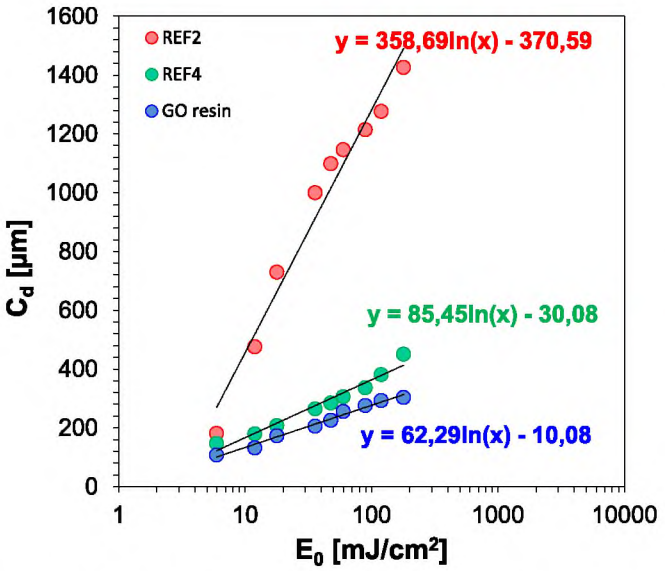

Fig. 5. Determined Jacob's basic working curves for resins: REF2, REF4 and GO resin.

Table 3
Calculated 3D printing characteristics for photo-curable resins: REF2, REF4 and GO resin.

3D printing parameters			
Resin	**Equation**	**Critical energy [mJ/cm^2]**	**Curing depth [µm]**
REF2	y = 358.69ln(x)-370.59	2.81	380.44
REF4	y = 85,45ln(x) – 30,08	1.42	82.22
GO resin	y = 62,29ln(x) – 10,08	1.17	62.80

which proves that the cross-linked material compared to GO resin 10 min. For the control materials, no significant differences in dimensions were observed depending on the curing time of the printout.

3.5.2. Mechanical analysis

Fig. 9 shows the mechanical properties of 3D printed nanocomposities for different curring times. According to the results, the Young's modulus of the final material increased slightly with post-curing time. This is due to the speed of the radical polymerization process, which occurs relatively quickly, which explains the slight differences in the mechanical properties depending on the curing time. A much greater effect on the mechanical properties of the material was observed during the polymer modification with nanoparticles. The incorporation of GO into polymer-based resins improved the mechanical properties of the final materials. GO exhibits excellent hydrophilic properties. This high hydrophilicity is due to oxygen-containing groups such as oxygen, hydroxyl (–OH), carbonyl (–CO-), carboxyl (–COOH), alkoxy, and epoxide, which are present on the basal planes and edges of GO [63]. Thus, GO can easily interact with polymers, thereby improving their mechanical properties [64]. For nanocomposites with TPO, the Young's modulus of the GO resin nanocomposites increased two times, and the most spectacular results were obtained for two-component systems based on an iodine salt and a sensitizer. Materials without nanoadditives exhibited very poor mechanical properties. The introduction of GO increases the mechanical properties to values similar to those of commercial TPO and pure monomer [65].

3.5.3. Thermal analysis

The thermal properties of REF1 and the GO resin nanocomposites were evaluated by TGA and DSC, respectively, and the corresponding data are presented in Fig. 10. The TGA results show that the PEGDA network is thermally stable up to 270 °C whereas it undergoes thermal degradation between 300 °C and 460 °C which signifies the decomposition temperature. A long post-curing time of 60 min reduces the thermal instability of the polymer compared to a short one, which implies slower decomposition kinetics because the final decomposition temperature remains the same. The post-curing time did not change the size of decay about 94 %. The decrease in stability was also confirmed by the onset temperature determined using tangents. The addition of GO to the sample subjected to long post-curing times (60 min) increased the thermal stability of the polymer. This may be related to the reaction of the polymer chains with GO during extended post-curing. The end of the decay (kinetics) and the size of the decay remained unchanged. The addition of GO to the polymer with a shorter post-curing time increases the decay rate. A certain difficulty is that the decay, in this case, reaches 102 %, perhaps this is due of the simultaneous deposition of decay products on the balance elements, which changes the reference point.

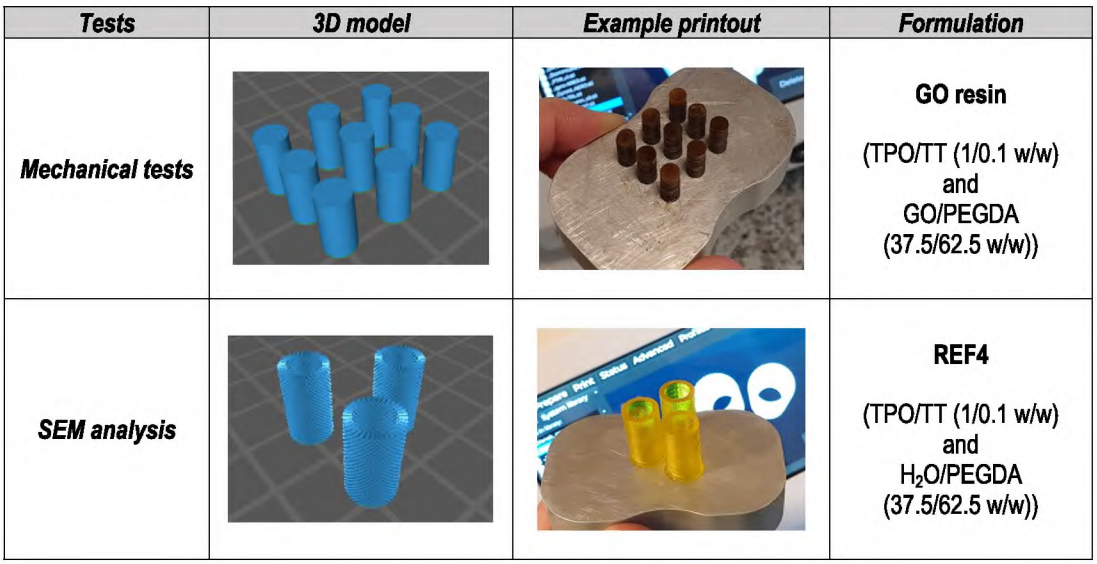

Fig. 6. 3D models for mechanical testing and SEM analysis with sample printouts.

Table 4
DLP 3D printing conditions for REF2, REF4 and GO resin.

3D printing conditions				
Resin	**Curing time of first layer [s]**	**Curing time of layers [s]**	**Thickness of the layer [μm]**	**Light intensity [mW/cm^2]**
REF2	3	1.5	100	2.98
REF4	6	3		
GO resin	6	2		

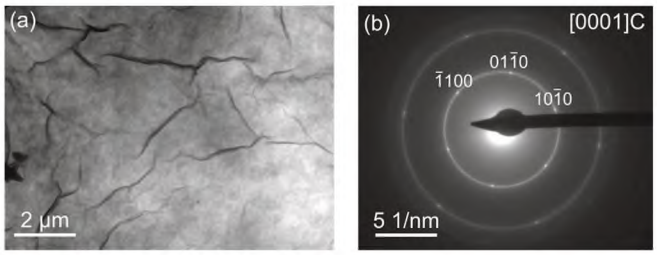

Fig. 7. TEM/BF microstructure image (a) and SAED pattern (b) obtained from the graphene oxide flake.

However, even assuming 100 %, it's still approximately 7 % more than without the addition of GO or with long post-curing time with the addition of GO. This indicates that there is a strong interaction between PEGDA and the GO nanofillers at the interface owing to the formation of hydrogen bonds. The chemical influence of GO, and probably C, on the bonded structure reacts with the post-curing process. This indicates a change in the mobility of the polymer chain at the borders, a decrease under the influence of long post-curing, and an increase again owing to the same post-curing but with the addition of GO.

4. New photo-curable nanoresin with novel initiator system

Because of the favorable results achieved by applying radical photopolymerization to the preparation of 3D printed nanocomposite materials using a radical initiator system, we decided to apply a two-component photoinitiator system for further research. GO-added nanoresin was prepared utilizing a new two-component initiator system based on bis-(4-t-butylphenyl)iodonium hexafluorophosphate and photosensitizer N-{4-[(E)-2-(pentafluorophenyl)ethenyl]phenyl}-2,1,3-benzothiadiazol-4-amine (IOD/PS1 1/1.0 w/w). The addition of the new initiator system to the nanoresin was aimed at eliminating the TPO initiator, which is a potentially toxic compound, making it unsuitable for biomedical applications. Creating a new two-component photoinitiating system that does not exhibit toxicity would greatly expand its application possibilities in the fields of medicine, dentistry, and tissue engineering. The research scheme was the same as that for resins with the free-radical initiator diphenyl (2,4,6-trimethyl benzoyl) phosphine oxide (TPO). The investigation began by verifying the spectroscopic properties of the newly synthesized PS1 compound. The synthetic procedure and confirmation of PS1 structure, are presented in the Supplementary Material (**S.1.**). Absorption measurements were performed in acetonitrile. The new compound absorbs radiation in the visible range, reaching up to 520 nm (Fig. 11), which is extremely promising in terms of its further application as a photosensitizer for iodonium salts using light sources in the visible range. However, one mechanism of photosensitization is based on electron transfer between the excited state of the photosensitizer and initiator in the ground state. By absorbing light quanta, the photosensitizer molecule is excited to a singlet state. The excited singlet states are characterized by very short lifetimes and are, therefore, transferred to the corresponding triplet states, which are characterized by longer lifetimes, making it possible to interact with molecules in the ground state. For this reason, electron transfer mainly occurs from the excited singlet and triplet states of the photosensitizer towards the initiator in the ground state. During this process, reactive forms capable of initiating polymerization are produced. The electron transfer photosensitization process depends on the thermodynamic conditions, the oxidation potential of the photosensitizer, and the reduction potential of the initiator.

Subsequently, two resin formulations were prepared: **REF5:** PS1/IOD (0.1/1 w/w) and PETIA/H_2O/PEGDA (30/26.25/43.75 w/w/w); **GO new resin:** PS1/IOD (0.1/1 w/w) and PETIA/GO/PEGDA (30/26.25/43.75 w/w/w). The PETIA monomer was added to the H_2O/PEGDA system employed in the previous chapter to act as a crosslinking agent. The formulated resins were examined kinetically (study of the kinetics of the radical photopolymerization process using infrared spectroscopy and photoreological investigations). Table 5 lists the parameters calculated from these measurements. Kinetic profiles obtained while measuring photopolymerization kinetics are included in Supplementary Material (**S.10.**).

The results obtained from kinetic measurements are very promising, despite the low over-reactivity of the acrylate groups for REF5 and GO new resin (at approximately 20 %). The conducted photorheological measurements showed that the gelation time of the new resin formulations was short and did not exceed 1 s, and the polymerization shrinkage was low (2 %), which is particularly relevant when it comes to the development of photo-curable polymer nanocomposites. The kinetic studies conducted were a precursor to application studies, where the new resin formulations were utilized as an input material for the 3D printing of objects using DLP technology. To properly carry out the 3D printing process, application studies began by determining the optimal printing parameters (the method of determining the critical energy and depth of light penetration were presented in the previous section). Fig. 12 represents Jacob's basic working curves obtained for the REF5 and GO new resin, while Table 6 shows the calculated 3D printing parameters.

Subsequently, an effort was made to obtain three-dimensional objects from the prepared resins using the new initiator system for SEM analysis (Fig. 13). As in the case of resins with a one-component initiator system in the form of TPO, REF5 and GO new resin also received prints, which in further stages were utilized for imaging by scanning electron microscopy. Compared to resins with TPO, for REF5 and GO new resin it was necessary to increase the exposure time for layers of printed objects and increase the intensity of light incident on the photo-curable resin during the 3D printing process. For the new GO resin prints, the layer thickness must be reduced to twice that of the REF5 resin print, which allows the photopolymerization process.. The 3D printing parameters of the new photo-cured nanoresins are listed in Table 7. However, despite the fact that the printing parameters of the new reference resin (REF 5) and the formulation with added graphene oxide (GO new resin) require much longer exposure times during the 3D printing process, this research shows that the employment of two-component photoinitiating systems based on an iodonium salt and an appropriately selected photosensitizer opens up entirely new possibilities for composing photo-curable formulations. In this chapter, we applied a two-component typical photoinitiating system based on an iodonium salt to initiate the radical photopolymerization process of acrylate monomers. However, it has been demonstrated that the selected initiating system enables the realization of works related to 3D printing of spatial objects. The possibility of applying this type of two-component photoinitiating system allows compositions with epoxy and vinyl monomers, which is

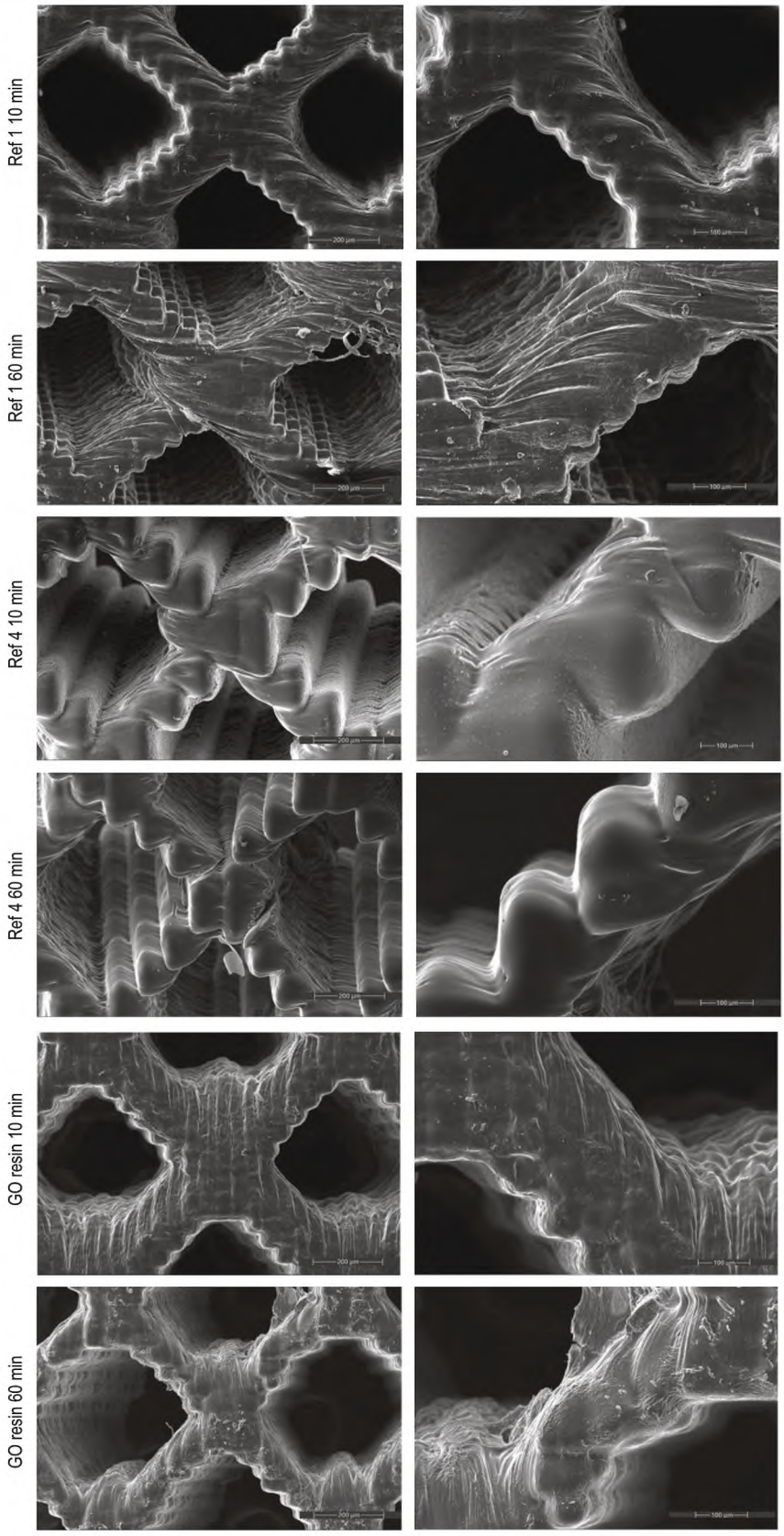

Fig. 8. SEM morphology of REF1, REF4, GO resin samples with different curing time: 10 and 60 min.

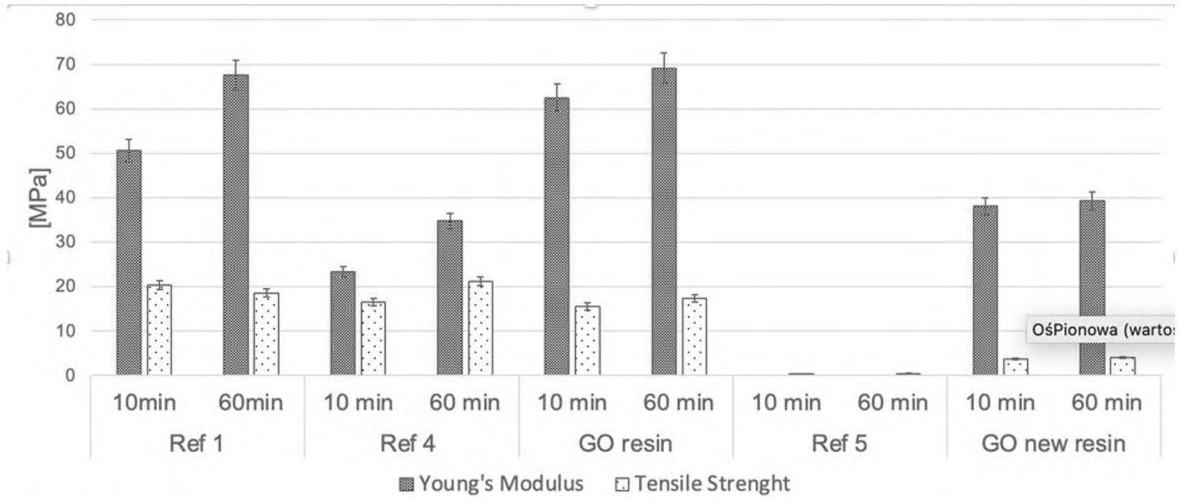

Fig. 9. Young's Modulus and Tensile Strenght of 3D printed nanocomposites: REF1, REF4, GO resin, REF5, GO new resin. GO nanoparticles incorporation into polymer matrix improves mechanical properties of final material.

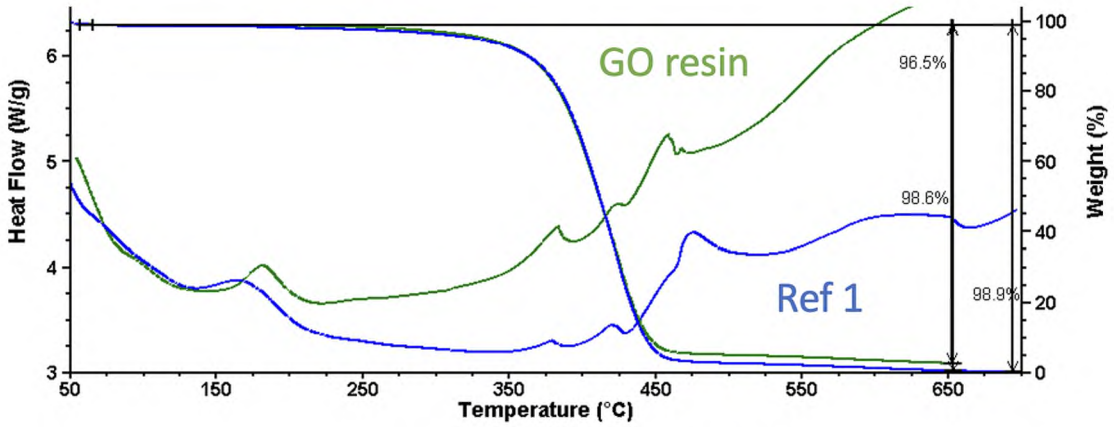

Fig. 10. TGA and DSC curves for REF1 and GO resin.

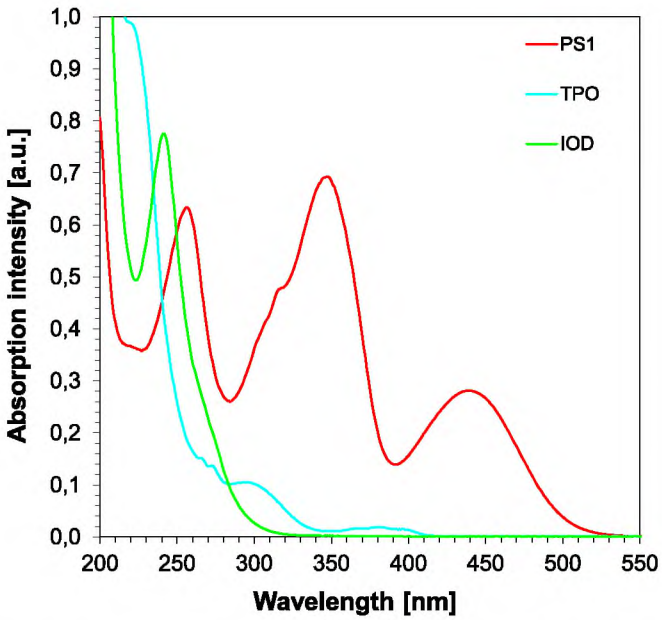

Fig. 11. Absorption characteristics of the individual components contained in the photoinitiating systems utilized in the investigated formulations.

Table 5
Kinetic parameters achieved for REF5 resin and GO new resin (Light intensity on photopolymerizing composition = 8.82 mW/cm^2).

Radical photopolymerization process kinetics FT-IR measurements		
Resin	**Formulation**	**Conversion [%]**
REF5	PS1/IOD (0.1/1 w/w) and PETIA/**H_2O**/PEGDA (30/26.25/43.75 w/w/w)	20
GO new resin	PS1/IOD (0.1/1 w/w) and PETIA/**GO**/PEGDA (30/26.25/43.75 w/w/w)	20

Photoreological measurements			
Resin	**Formulation**	**Gel time [s]**	**Polymerization shrinkage [%]**
REF5	PS1/IOD (0.1/1 w/w) and PETIA/**H_2O**/PEGDA (30/26.25/43.75 w/w/w)	0.20	2
GO new resin	PS1/IOD (0.1/1 w/w) and PETIA/**GO**/PEGDA (30/26.25/43.75 w/w/w)	0.90	2

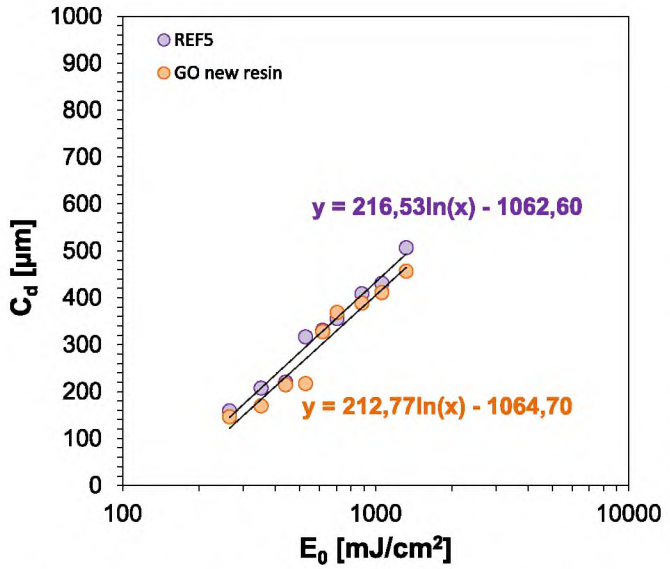

Fig. 12. Determined Jacob's basic working curves for resins: REF5 and GO new resin.

Table 6
Calculated 3D printing characteristics for photo-curable resins: REF5 and GO new resin.

3D printing parameters			
Resin	**Equation**	**Critical energy [mJ/cm²]**	**Curing depth [µm]**
REF5	y = 216.53ln(x)-1062.60	135.29	218.54
GO new resin	y = 212.77ln(x)-1064.70	149.01	223.86

typical of cationic photopolymerization, to be employed for composing formulations for 3D printing. This is due to the fact that the use of a two-component system based on an iodonium salt and a photosensitiser guarantees the generation not only of reactive radicals necessary for the initiation of radical photopolymerization, but also of radical-cations responsible for the photoinitiation of the ring-opening cationic polymerization process and the chain photopolymerization of vinyl monomers.

The SEM morphologies of the materials with the new initiator system at different curing times are shown in Fig. 14. According to the results, the images in REF5 showed imperfections that appeared as cracks. Individual layers were clearly visible regardless of the curing time. Resins may not be cured uniformly or may have inconsistencies in their composition, which can result in visible layer lines in the final print [66]. Resin with GO nanoparticles, on the other hand, tends to have more uniform curing properties, resulting in a smoother surface finish and less visible layer lines. This proves that the GO nanoparticles are evenly dispersed throughout the resin without clumping or aggregation, which can lead to uneven curing and visible layer lines in the final print. The formation of cracks in materials printed using additive manufacturing with GO nano fillers can be attributed to poor dispersion and agglomeration of GO nanoparticles. If the GO nanoparticles are not well-dispersed in the matrix, this can lead to regions of weak bonding between the filler and the matrix, causing cracks propagation. Additionally, agglomeration or clustering of GO nanoparticles can create stress concentrations within the material, leading to the development of cracks [67]. Moreover, some initiator systems, like TPO, can be sensitive to oxygen inhibition, which may result in incomplete polymerization and crack propagation [68]. The specific combination of bis-(4-t-butylphenyl)iodonium hexafluorophosphate and photosensitizer N-{4-[(E)-2-(pentafluorophenyl)ethenyl]phenyl}-2,1,3-benzothiadiazol-4-amine promotes a more controlled and uniform polymerization process, resulting in reduced shrinkage-induced stresses and better interlayer bonding. The photosensitizer in the initiator system efficiently absorbs UV light and facilitates the initiation process, leading to a more uniform cure throughout the material. According to the results, the novel two-component initiator system provided an innovative and effective approach. Its unique chemical structure facilitated strong interactions with functional groups present on the GO surface, reducing agglomeration and promoting a homogeneous distribution throughout the composite. Graphene oxide has a large surface area and contains various oxygen-containing functional groups like epoxides, hydroxyls, and carboxylic acids. The functional groups on GO can engage in hydrogen bonding and other non-covalent interactions, such as van der Waals forces, with a wide variety of substances. Iodonium salts are positively charged, and their non-polar sections might be attracted to the carbon backbone of the GO. The van der Waals interactions can occur between the aromatic rings of the iodonium salt and the aromatic structure of graphene in the GO. What is more, The iodonium salt could potentially interact with negatively charged sites on the GO surface, leading to an electrostatic interaction that stabilizes the dispersion of the GO nanoparticles within the resin matrix. In summary, the proposed interactions between GO and bis-(4-t-butylphenyl)iodonium hexafluorophosphate are plausible based on the known chemistry of these compounds. These interactions might be instrumental in the dispersion of GO within the resin as confirmed by the absence of cracks in the final printouts. However, for the GO new resin samples, many voids were visible in the

Table 7
DLP 3D printing conditions for REF5 and GO new resin.

3D printing conditions				
Resin	**Curing time of first layer [s]**	**Curing time of layers [s]**	**Thickness of the layer [µm]**	**Light intensity [mW/cm²]**
REF5	150	30	100	8.82
GO new resin	150	30	50	

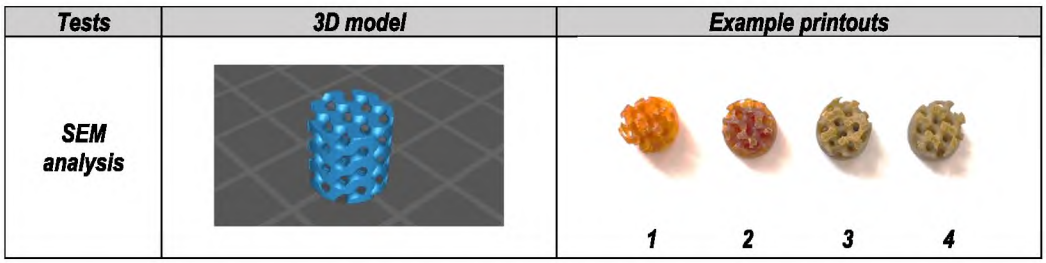

Fig. 13. 3D models for SEM analysis with sample printouts (1 – REF5, 10 min postcuring; 2 - REF5, 60 min postcuring; 3 – GO new resin, 10 min postcuring; 4 – GO new resin, 60 min postcuring).

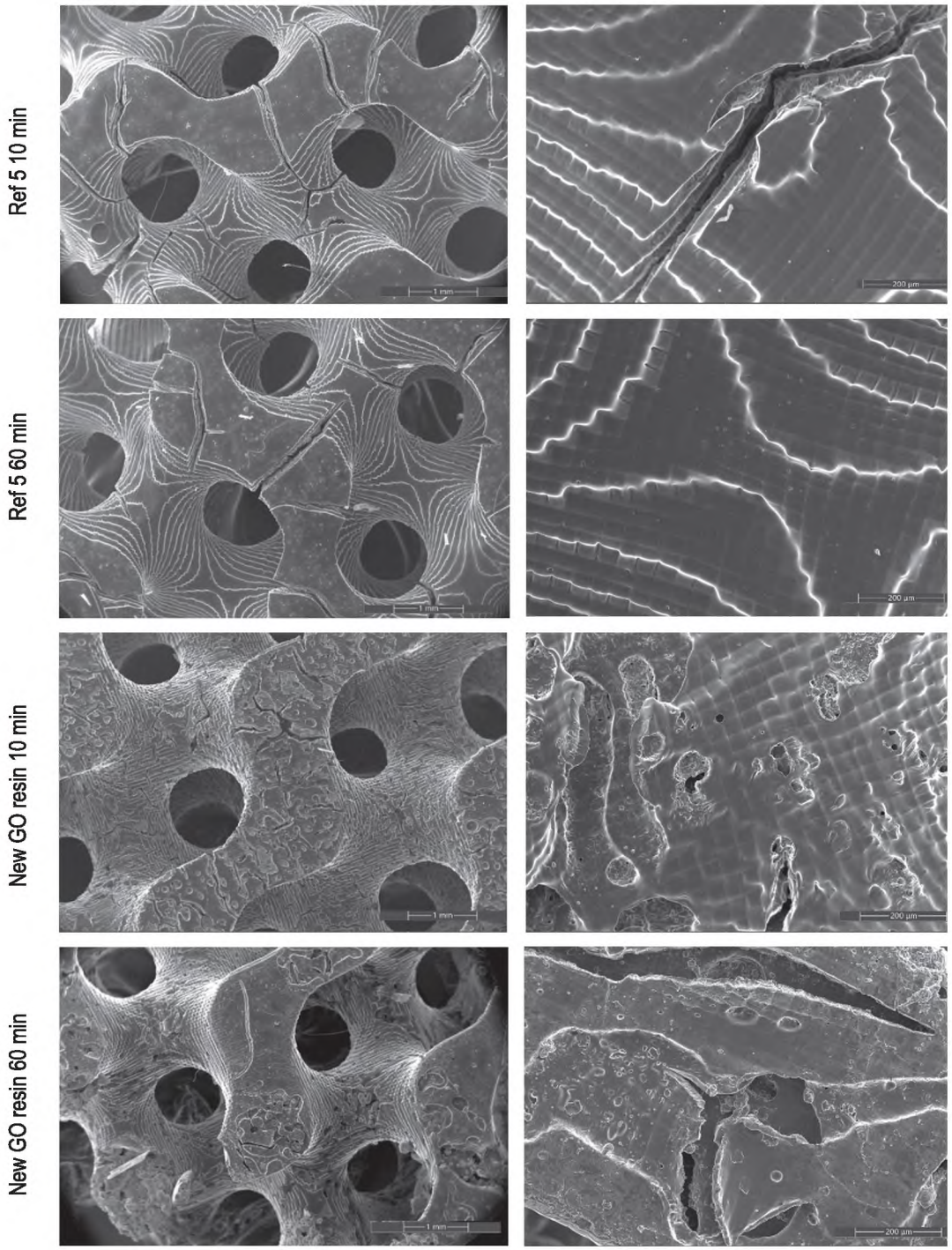

Fig. 14. SEM morphology of REF5 and GO new resin materials with different curing time: 10 and 60 min.

final printouts. To minimize these imperfections, it is important to optimize printing parameters, such as exposure time and layer thickness, to achieve the best possible results. Additionally, it may be necessary to use a higher concentration of GO particles or to modify the printing parameters to achieve the desired mechanical properties without introducing imperfections [69–70]. Nevertheless, the analyses carried out indicate the high potential of the new initiating system for the 3D printing of materials with high-performance properties.

5. Conclusions

In response to the need for a more versatile and environmentally friendly initiating system for photopolymerization processes, especially for incorporating GO nanoparticles into the resin matrix, this study led to the creation of a novel two-component initiator system. This innovative system, comprised of bis-(4-t-butylphenyl)iodonium hexafluorophosphate and photosensitizer N-{4-[(E)-2-(pentafluorophenyl) ethenyl]phenyl}-2,1,3-benzothiadiazol-4-amine (IOD/PS1), was specifically formulated to expand applicability to radical, cationic, and hybrid photopolymerizations. The PS1 component's absorption capabilities up to a wavelength of approximately 520 nm provide a substantial advantage over TPO, broadening the range of suitable light sources for photopolymerization initiation.

In this study, the innovative applications of 3D printing with light-

initiated technologies were explored, specifically focusing on the incorporation of GO nanoparticles into photopolymerizing resins. The inclusion of GO nanoparticles in the resin matrix yielded enhanced mechanical, thermal, and conductive characteristics in the final printed structures, broadening the potential applications in various scientific fields. The study focused on optimizing the dispersion of GO nanoparticles within the resin matrix. Traditional methods were examined, but the novel two-component initiator system emerged as an effective approach. Its unique chemical structure facilitated strong interactions with the functional groups on the GO surface, reducing agglomeration and promoting a homogeneous distribution throughout the composite. This not only improved mechanical and thermal stability but also minimized stress concentrations, thereby reducing the propensity for crack formation.

CRediT authorship contribution statement

Klaudia Trembecka-Wójciga: Conceptualization, Data curation, Formal analysis, Investigation, Validation, Visualization, Writing – original draft, Writing – review & editing. **Magdalena Jankowska:** Data curation, Formal analysis, Investigation, Validation, Visualization, Writing – original draft, Writing – review & editing. **Wiktoria Tomal:** Data curation, Formal analysis, Investigation, Funding acquisition. **Anna Jarzębska:** Data curation, Investigation. **Łukasz Maj:** Data curation, Investigation. **Tomasz Czeppe:** Data curation, Investigation. **Paweł Petrzak:** Data curation, Investigation. **Anna Chachaj-Brekiesz:** Data curation, Investigation, Visualization. **Joanna Ortyl:** Conceptualization, Methodology, Project administration, Funding acquisition, Resources, Validation, Writing – review & editing, Supervision.

Declaration of Competing Interest

The authors declare that they have no known competing financial interests or personal relationships that could have appeared to influence the work reported in this paper.

Data availability

Data will be made available on request.

Acknowledgments

The present research work was funded by the OPUS LAP project contract number 2020/39/I/ST5/03556 “Advanced photopolymerized nanocomposite materials processed by additive manufacturing.” funded by National Science Center.

The publication (open access cost of publication) was funded by the project “ROAD TO EXCELLENCE - a comprehensive university support programme” implemented under the Operational Programme Knowledge Education Development 2014-2020 co-financed by the European Social Fund; agreement no. POWR.03.05.00-00-Z214/18, moreover one of the author (W. T.), would like to thank this project for the financial support of the investigator.

Appendix A. Supplementary material

Supplementary data to this article can be found online at https://doi.org/10.1016/j.eurpolymj.2023.112403.

References

[1] Y. Wang, Y. Wang, C. Mao, D. Mei, Mater. Des. 227 (2023), 111698.
[2] T. Rehbein, A. Lion, M. Johlitz, A. Constantinescu, Polym. Test. 83 (2020), 106356.
[3] C.I. Higgins, T.E. Brown, J.P. Killgore, Addit. Manuf. 38 (2021), 101744.
[4] W. Tomal, H.C. Kiliclar, P. Fiedor, J. Ortyl, Y. Yagci, Macromol. Rapid Commun. 44 (2023) 3.
[5] M. Layani, X. Wang, S. Magdassi, Adv. Mater. (2018) 30.
[6] E. Hola, J. Ortyl, M. Jankowska, M. Pilch, M. Galek, F. Morlet-Savary, B. Graff, C. Dietlin, J. Lalevée, Polym. Chem. 11 (2020) 922–935.
[7] D.L. Naik, R. Kiran, Addit. Manuf. 23 (2018) 181–196.
[8] A. Al Rashid, W. Ahmed, M.Y. Khalid, M. Koç, Addit. Manuf. 47 (2021).
[9] W. Tomal, M. Pilch, A. Chachaj-Brekiesz, J. Ortyl, Catalysts (2019) 9.
[10] D. Gan, L. Han, M. Wang, W. Xing, T. Xu, H. Zhang, K. Wang, L. Fang, X. Lu, ACS Appl. Mater. Interfaces 10 (2018) 36218–36228.
[11] C. Zhu, C. Ninh, C.J. Bettinger, Biomacromolecules 15 (2014) 3474–3494.
[12] W. Tomal, A. Chachaj-Brekiesz, R. Popielarz, J. Ortyl, RSC Adv. 10 (2020) 32162–32182.
[13] W. Tomal, D. Krok, A. Chachaj-Brekiesz, J. Ortyl, Eur. Polym. J. 156 (2021), 110603.
[14] Z. Quan, A. Wu, M. Keefe, X. Qin, J. Yu, J. Suhr, J.H. Byun, B.S. Kim, T.W. Chou, Mater. Today 18 (2015) 503–512.
[15] K. Jlassi, S. Chandran, M. Mičušik, M. Benna-Zayani, Y. Yagci, S. Thomas, M. M. Chehimi, Eur. Polym. J. 72 (2015) 89–101.
[16] C. Ingrosso, C. Esposito Corcione, R. Striani, R. Comparelli, M. Striccoli, A. Agostiano, M.L. Curri, M. Frigione, ACS Appl. Mater. Interfaces 7 (2015) 15494–15505.
[17] X. Zheng, D. Wu, T. Su, S. Bao, C. Liao, Q. Wang, ACS Appl. Mater. Interfaces 6 (2014) 19840–19849.
[18] V.S. Vo, S. Mahouche-Chergui, V.H. Nguyen, S. Naili, B. Carbonnier, ACS Sustain. Chem. Eng. 7 (2019) 15211–15220.
[19] Z. Czech, A. Kowalczyk, J. Ortyl, J. Swiderska, Pol. J. Chem. Technol. 15 (2013) 12–14.
[20] M. Shah, A. Ullah, K. Azher, A. Ur Rehman, W. Juan, N. Aktuřk, C.S. Tufekcig, M. U. Salamci, RSC Adv. 13 (2023) 1456–1496.
[21] Q. Mu, L. Wang, C.K. Dunn, et al., Addit. Manuf. 18 (2017) 74–83.
[22] M. Topa, F. Petko, M. Galek, M. Jankowska, R. Popielarz, J. Ortyl, Eur. Polym. J. 156 (2021), 110612.
[23] S.L. de Armentia, S. Fernández-Villamarín, Y. Ballesteros, J.C. Del Real, N. Dunne, E. Paz, Int. J. Bioprint 8 (2022) 503.
[24] E. Hola, M. Pilch, M. Galek, J. Ortyl, Polym. Chem. 11 (2020) 480–495.
[25] Y. Li, D. Pan, S. Chen, Q. Wang, G. Pan, T. Wang, Mater. Des. 47 (2013) 850–856.
[26] W. Tomal, J. Ortyl, Eur. Polym. J. 2022 (2022) 180.
[27] E. Hola, M. Topa, A. Chachaj-Brekiesz, M. Pilch, P. Fiedor, M. Galek, J. Ortyl, RSC Adv. 10 (2020) 7509–7522.
[28] M. Lang, S. Hirner, F. Wiesbrock, P. Fuchs, Polymers 14 (2022) 2074.
[29] J. Ortyl, J. Wilamowski, P. Milart, M. Galek, R. Popielarz, Polym. Test. 48 (2015) 151–159.
[30] M. Topa, J. Ortyl, A. Chachaj-Brekiesz, I. Kamińska-Borek, M. Pilch, R. Popielarz, Spectrochim. Acta A Mol. Biomol. Spectrosc. 199 (2018) 430–440.
[31] M. Topa, E. Hola, M. Galek, F. Petko, M. Pilch, R. Popielarz, F. Morlet-Savary, B. Graff, J. Laleveé, J. Ortyl, Polym. Chem. 11 (2020) 5261–5278.
[32] M. Topa, J. Ortyl, Materials 13 (2020) 18.
[33] S. Zakeri, M. Vippola, E. Levänen, Addit. Manufac. 35 (2020), 101177.
[34] J. Ortyl, K. Sawicz, R. Popielarz, J. Polym. Sci. A Polym. Chem. 48 (2010) 4522–4528.
[35] E. Hola, M. Pilch, J. Ortyl, Catalysts 10 (2020) 1–28.
[36] M.M. Hanon, A. Ghaly, L. Zsidai, S. Klébert, Mater. Des. 218 (2022), 110718.
[37] M.M. Hanon, A. Ghaly, L. Zsidai, Z. Szakál, I. Szabó, L. Kátai, Acta Polytech. HungVol. 18 (2021) 8.
[38] S.S.A. Kumar, N. Badawi M., K. M. Batoo, I. A. W. Ma, K. Ramesh, S. Ramesh and M. A. Shah, Sci Rep 2023, 13, 8946.
[39] A. Chiappone, I. Roppolo, E. Naretto, Er. Fantino, F. Calignano, M. Sangermano, F. Pirri, Compos B Eng, 2017, 124, 9-15.
[40] O. Ajiteru, M.T. Sultan, Y.Y. Lee, Y. Seo, H. Hong, J.S. Lee, C.H. Park, Nano Lett. 20 (2020) 6873–6883.
[41] Y. Zare, K.Y. Rhee, D. Hui, Composites Part B: Eng 122 (2017) 41–46.
[42] Y. Liang, D. Wu, X. Feng, K. Müllen, Adv. Mater. 21 (2009) 1679–1683.
[43] J.P., Edaugal, E.L. Ribeiro, M.K. Mitchell, MRS Communications 2023.
[44] Z.S. Pour, M. Ghaemy, Compos. Sci. Technol. 136 (2016) 145–157.
[45] F. Fang, S. Ran, Z. Fang, Compos. B Eng. 165 (2019) 406–416.
[46] M.T.H. Nguyen, S.Y. Kim, T.H. Jeong, Electron. Mater. Lett. 18 (2022) 275–281.
[47] S. Guo, Y. Lu, X. Wan X, Cem Concr Compos. 2020, 105, 103424.
[48] Z.S. Pour, Ghaemy M, Compos. Sci. Technol. 136 (2016) 145–157.
[49] M. Sandhya, D. Ramasamy, K. Sudhakar, K. Kadirgama, W.S.W. Harun, Ultrason. Sonochem. 73 (2021), 105479.
[50] A.S. Al-Asadi, Q.M. Hassan, A.F. Abdulkader, Opt. Mater. 89 (2019) 460–467.
[51] U. Kilic, M.M. Sherif, O.E. Ozbulut, Polym. Test. 76 (2019) 181–191.
[52] X. Wang, F. Tang, X. Qi, Compos. B Eng. 176 (2019), 107103.
[53] G.T. Kim, H.B. Go, J.H. Yu, S.Y. Yang, K.M. Kim, S.H. Choi, J.S. Kwon, Polymers 14 (2022) 979.
[54] M. Popal, J. Volk, G. Leyhausen, W. Geurtsen, Dent. Mater. 34 (2018) 1783–1796.
[55] F. Dumur, Europ. Polym. J. 169 (2022) 2.
[56] M. Jankowska, A. Chachaj-Brekiesz, K. Trembecka-Wójciga, A. Jarzębska, M. Topa-Skwarczyńska, M. Pilch, J. Ortyl, Polym. Chem. 14 (2023) 2088–2106.
[57] W. Tomal, D. Krok, A. Chachaj-Brekiesz, P. Lepcio, J. Ortyl, Addit. Manuf. 48 (2021), 102447.
[58] S. Asmussen, W. Schroeder, I. Dell'Erba, C. Vallo, Polym. Test. 32 (2013) 1283–1289.
[59] W. Tomal, M. Pilch, A. Chachaj-Brekiesz, M. Galek, F. Morlet-Savary, B. Graff, C. Dietlin, J. Lalevée, J. Ortyl, Polym. Chem. 11 (2020) 4604–4621.
[60] D.A. Rau, J.P. Reynolds, J.S. Bryant, M.J. Bortner, C.B. Williams, Addit. Manuf. 60 (2022), 103207.
[61] J. Bennett, Addit. Manuf. 18 (2017) 203–212.

[62] B. Steyrer, B. Busetti, G. Harakály, R. Liska, J. Stampfl, Addit. Manuf. 21 (2018) 209–214.
[63] I.K. Moon, J. Lee, R.S. Ruoff, H. Lee, Nat. Commun. 1 (2010) 6.
[64] S. J. Lee, S. J. Yoon and I. Y. Jeon, Polymers (Basel), 2022, 14.
[65] S.Y. Hong, Y.C. Kim, M. Wang, H.I. Kim, D.Y. Byun, J. Do Nam, T.W. Chou, P. M. Ajayan, L. Ci, J. Suhr, Polymer (Guildf) 145 (2018) 88–94.
[66] A.S. Alketbi, Y. Shi, H. Li, A. Raza, T.J. Zhang, Soft Matter 17 (2021) 7188–7195.
[67] M. Shah, A. Ullah, K. Azher, A. Ur Rehman, N. Akturk, W. Juan, C.S. Tüfekci, and M.U. Salamci, Crystalsm, 2023, 13, 285.
[68] G. Xie, Z. Shuai, Y. Huang, M. Yu, Z. Zeng, J. Yang, Prog. Org. Coat. 147 (2020), 105716.
[69] H. Gojzewski, Z. Guo, W. Grzelachowska, M.G. Ridwan, M.A. Hempenius, D. W. Grijpma, G.J. Vancso, ACS Appl. Mater. Interfaces 12 (2020) 8908–8914.
[70] S.J. Paulsen, T.M. Mitcham, C.S. Pan, J. Long, B. Grigoryan, D.W. Sazer, C. J. Harlan, K.D. Janson, M.D. Pagel, J.S. Miller, R.R. Bouchard, PLoS One 16 (2021) 12.